Optics Letters

Divided-pulse amplification to the joule level

Benjamin Webb,[1] Ahmad Azim,[1] Nathan Bodnar,[1] Michael Chini,[1,2] Lawrence Shah,[1,*] and Martin Richardson[1]

[1]Townes Laser Institute, College of Optics and Photonics, University of Central Florida, 4000 Central Florida Blvd., Orlando, Florida 32816, USA
[2]Department of Physics, University of Central Florida, 4000 Central Florida Blvd., Orlando, Florida 32816, USA
*Corresponding author: lshah@creol.ucf.edu

Received 23 March 2016; revised 2 June 2016; accepted 6 June 2016; posted 6 June 2016 (Doc. ID 261814); published 30 June 2016

Divided-pulse amplification (DPA) has proven to be a valuable tool in scaling the peak power of diode-pumped ytterbium-doped amplifiers to beyond the single-pulse threshold for parasitic nonlinear effects. DPA enables the amplification of picosecond pulses in solid-state amplifiers with limited bandwidth beyond the single-pulse damage threshold. In this Letter, we demonstrate DPA of picosecond pulses in a flashlamp-pumped Nd:YAG amplifier for the first time, to the best of our knowledge, yielding a combined pulse energy of 167 mJ.

OCIS codes: (140.3280) Laser amplifiers; (140.3298) Laser beam combining; (140.3530) Lasers, neodymium; (140.3580) Lasers, solid-state; (140.7090) Ultrafast lasers.

http://dx.doi.org/10.1364/OL.41.003106

Nonlinear effects and optical damage fundamentally constrain the amplification of time-bandwidth-limited picosecond pulses. The invention of chirped-pulse amplification (CPA) circumvents these limitations for femtosecond pulses by using dispersion to spectrally stretch the pulse in time to hundreds of picoseconds. However, CPA becomes cumbersome, if not impossible, for transform-limited pulses with durations greater than a few picoseconds, due to the cost of large aperture gratings and system footprint constraints. The need for energy-scalable picosecond lasers to pump optical parametric chirped-pulse amplification (OPCPA) [1,2] has driven the development of additional methods to reduce intensity during amplification and operate near the saturation fluence of the laser gain media for efficient energy extraction.

One promising method to artificially stretch the duration of picosecond pulses is via divided-pulse amplification (DPA) [3], also referred to as coherent pulse addition. Strictly speaking in DPA, a pulse is divided into several replicas that are delayed in time to avoid damage and nonlinear effects during amplification. However, conceptually and practically, this is closely related to coherent beam combination (CBC) in which the pulse replicas are separated spatially in parallel amplifiers. In both cases, after amplification, the pulse replicas are coherently combined into a single higher energy pulse. Furthermore, both DPA and CBC can be implemented together and share similar challenges relative to managing the pulse division, amplification, and recombination. To date, DPA and CBC of ultrashort pulses have primarily been applied to fiber or fiber-like solid-state amplifiers. The combination of CBC with CPA in a ytterbium (Yb) fiber system allowed energy scaling up to 5.7 mJ with 22 GW peak power [4], well beyond the limit of CPA alone [5].

After the first demonstration of DPA [6], a variety of pulse-splitting methods have been incorporated into DPA and CBC, including birefringent crystal stacks [3] and interferometers with Sagnac [7], Mach–Zehnder [8], and Gires–Tournois [9] configurations. The combination efficiency of passively stable DPA techniques, where a single interferometer or element is used for both pulse division and recombination, is inherently limited by gain saturation and B-integral variation across the amplified replicas [10]. The effects of gain saturation can be compensated for to some degree by using a combiner that is separate from the splitter. However, this requires active stabilization of the optical paths of each pulse replica, and, therefore, is referred to as active DPA. Since DPA is a form of CBC, established methods for phase locking can be utilized for active stabilization. Feedback from a Hänsch–Couillaud (HC) [11,12] detector to a piezoelectric mirror in each splitting interferometer has been the most common implementation in active DPA, although single detector methods such as LOCSET offer the ability to phase lock a large number of pulse replicas [13,14].

Ideal pulse recombination requires that the pulses be identical in temporal shape, phase, and spatial profile, as well as perfectly overlapped in space and time. Due to the stringent requirements on beam quality, repeatability, and stability, nearly all DPA demonstrations to date have exploited ytterbium-doped fiber laser systems or hybrid fiber-bulk systems [15,16]. The only non-fiber demonstration of DPA passively combined two pulses after multi-pass amplification in a Yb:CaF_2 rod, yielding a single 160 mJ pulse [17]. Although the majority of DPA and pulsed CBC systems have focused on a coherent combination of Gaussian beam profiles, efficient combination of other profile shapes is achievable, as long as replicas remain identical in wavefront and energy distribution [18].

To scale DPA to joule energy and kW average power, it has been proposed to develop an enhancement cavity together with

the combined output of >16 fiber lasers, enabling simultaneous scaling of average power and energy [19]. This Letter investigates an alternative approach using flashlamp-pumped Nd:YAG rod amplifiers, demonstrating the utility of DPA for non-Gaussian beam profiles and pulsed pump configurations. While this approach is limited to relatively low repetition rates, the laser technology is widespread, and single beamline energy at the kilojoule level has been demonstrated via Nd-doped phosphate glass amplifiers [20,21]. Furthermore, the average power and overall efficiency of this approach could be further improved by implementing large-aperture pulse diode-pumped solid-state amplifiers which have recently reached the joule level [22–24].

Efficient energy extraction is key for realizing DPA at the joule level and beyond. Efficient energy extraction requires that amplifiers be operated well above the saturation fluence; however, for picosecond pulses the damage threshold of most gain media is below the saturation fluence. Due to its four-level laser nature, Nd:YAG has a very low saturation fluence (~0.6 J/cm^2) compared to Yb-doped media (~10 J/cm^2). The high gain of Nd:YAG also reduces the accumulation of the B-integral phase, since transmission through less amplifier material is required to reach a particular energy. In short, the properties of Nd:YAG including accessibility, low saturation fluence, high gain, and non-birefringence are well suited for high energy DPA.

This Letter demonstrates active DPA in a flashlamp-pumped Nd:YAG amplifier chain for the first time, to the best of our knowledge, with active stabilization accomplished via a co-propagating continuous-wave (CW) laser. A record combined pulse energy of 167 mJ (527 mJ equivalent) is achieved with 230 ps pulse duration, as well as demonstrating DPA well above the gain saturation fluence for the first time, to the best of our knowledge.

The Nd:YAG DPA system (Fig. 1) is seeded at 1064 nm by a portion of the energy from an octave-spanning 5 fs pulsed Ti:sapphire oscillator (Idesta-QE), to ensure optical synchronization with a future high-energy optical parametric chirped-pulse amplification (OPCPA) system. The seed spectrum is filtered by a narrow bandwidth volume Bragg grating (VBG) inside an Nd:YAG regenerative amplifier to adjust the transform-limited pulse duration to 230 ps with an amplified

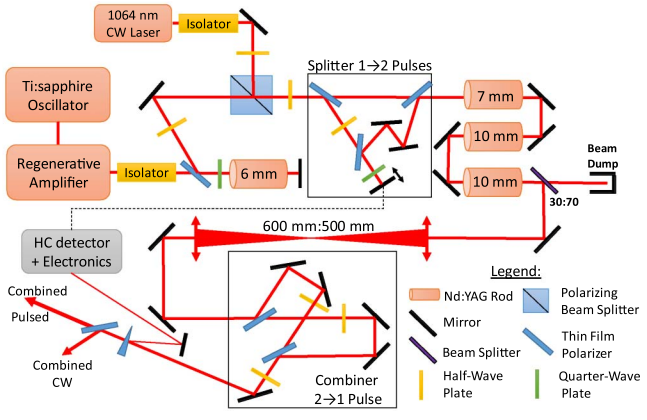

Fig. 1. Design of a flashlamp-pumped Nd:YAG DPA system actively stabilized by CW laser feedback to a Hänsch–Couillaud (HC) detector.

energy of 0.3 mJ at 2.5 Hz [25]. The regenerative amplifier output passes through a Faraday isolator prior to double-pass amplification to 8 mJ in a 6 mm diameter rod. The pulse is then divided into two replicas separated by a time delay of ~750 ps. To minimize back reflected energy to the double-pass amplifier, the Mach–Zehnder-type pulse splitter includes an extra thin-film polarizer (TFP) just before the zero-degree piezo-mounted mirror utilized for active stabilization. Transmission through the extra polarizer not only improves the polarization contrast of the reflected replica from the first polarizer, but also minimizes back reflected energy to ~0.5%.

Next, the two pulse replicas are amplified in a series through one 7 mm and two 10 mm diameter rods to a total energy of 625 mJ. Due to the aperture and damage threshold limitation imposed by the 14 mm × 28 mm rectangular TFPs in the pulse combining stage, the energy in the combiner was limited to ~200 mJ. Hence, ~70% of the total energy was directed to a beam dump through a beam splitter. The design of the high-energy pulse combiner eliminates folded paths so as to avoid back reflection, since there is no way to isolate between the high gain amplifiers and the combiner without division of the orthogonally polarized replicas into spatially separated channels. The unique design of the pulse combiner maximizes system efficiency with the use of high transmission (>98%) TFPs and operation of all mirrors with s-polarized light at 45 deg incidence. Each replica is transmitted through a single polarizer to enhance polarization contrast before coherent combination. This design is well suited for energy scaling DPA to the joule level and beyond since TFPs with high transmission, high damage threshold, and sufficiently large aperture are available.

To actively stabilize the optical path difference (OPD) of the pulse replicas, the error signal from a Hänsch–Couillaud (HC) detector [11,24] is fed back to a zero-degree mirror mounted to a piezoelectric transducer in the reflected path of the pulse splitter. Given the low repetition rate of the laser itself, we chose to stabilize the OPD using a co-propagating CW beam. By injecting a CW 1064 nm laser into the pulsed beam path from a polarizer just before the splitter (Fig. 1), two beams share the same divided paths through to the combiner. Since the polarization of the CW beam before the splitter is orthogonal to the pulses, the final combined CW output will be reflected from the analyzing polarizer while the combined pulses are transmitted. Sampling of the beam is accomplished with an AR-coated wedge placed just after the beams are combined, but before the analyzing polarizer. The sampled beam is sent to the HC detector consisting of a QWP followed by a polarizer with a photodiode at each output. The difference signal from the photodiodes is fed into a proportional-integral (PI) control loop in LabVIEW. An Arduino Uno circuit is used to read the photodiode signals into LabVIEW and generate a pulse-width-modulation (PWM) output signal, which is low-pass filtered before amplification by the piezo-mirror driver circuit. While the PI control in LabVIEW can have a 1 ms loop time, we have found that we can effectively suppress the high-frequency noise by minimizing the coupling of vibration sources to the optical table. The PI loop and piezo mirror then compensate the remaining low-frequency noise (Fig. 2).

The output energy fluctuates by >40% without active stabilization due to phase errors >1 rad (Fig. 2). Active stabilization using the CW beam reduces the amplitude of phase

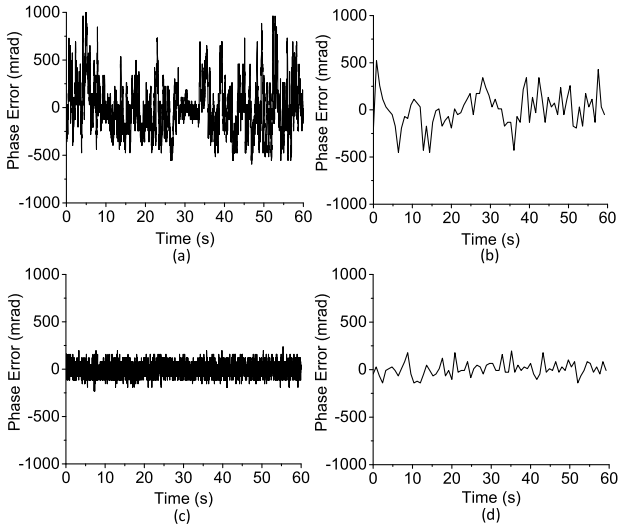

Fig. 2. Phase fluctuation measured in the combined output over 60 s (a) CW free-running, (b) pulsed free-running, (c) CW phase-locked, and (d) pulsed while phase-locked from CW feedback.

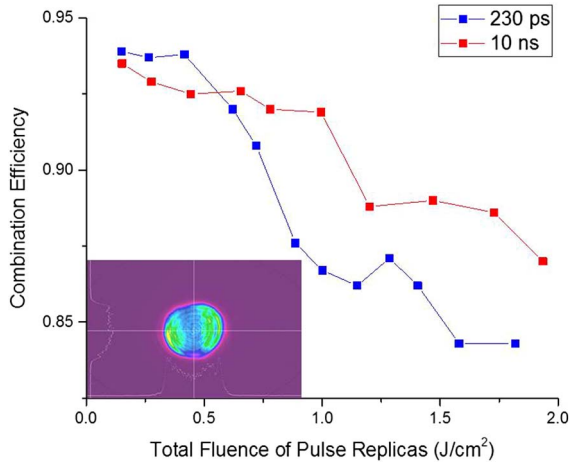

Fig. 3. For 10 ns and 230 ps pulses, the combination efficiency is recorded versus the sum fluence of two pulse replicas at the output of the final amplifier. The inset shows the combined 230 ps beam profile.

fluctuations in the pulsed output to ~90 mrad rms [Fig. 2(d)], corresponding to an energy fluctuation of 0.4% rms since the output of an interferometer is related to the cosine function [12]. An rms phase error of 58 mrad was measured over 60 s for the CW beam, corresponding to a power fluctuation of less than 0.2% rms [Fig. 2(c)]. Synchronized triggering of the HC electronics allowed for measurement of the CW and 2.5 Hz-pulsed phase errors. The output energy fluctuation of this system is acceptable, since most commercial flashlamp-pumped Nd:YAG lasers specify energy stabilities of greater than 1% rms.

Given that perfect pulse recombination requires identical replicas, variations induced by non-uniform B-integral, gain saturation, and other effects in the amplifiers degrade combination efficiency at high energy. The combination efficiency was plotted with respect to the total fluence of the two pulse replicas in Fig. 3. To the best of our knowledge, a record combined energy of 167 mJ was achieved for a 230 ps pulse with a maximum amplifier fluence ~3 times the saturation fluence (~0.6 J/cm^2) (Fig. 3). Due to limited aperture combiner optics, ~30% of the total amplifier energy is sampled and sent directly to the combiner (Fig. 1). A combined energy of 527 mJ could be realized with larger polarizers, since B-integral and saturation effects are unchanged by a scaled-aperture combiner. Work on a second generation DPA system with 60 mm aperture polarizers is under way. Combination efficiency up to 94% was measured for pulses at half the saturation fluence. The combination efficiency dropped to 84% at three times the saturation fluence for a combined energy of 167 mJ (sampled from the 625 mJ amplifier output). The combination efficiency was measured by the ratio of the energy after the analyzing polarizer to the sum energy of the pulses just before the polarizer. If the scattering loss of the polarizer is considered negligible, this measurement is equivalent to the ratio of energy transmitted to sum energy of both polarizer outputs. The system efficiency at maximum energy is 78.4%, including the combination efficiency, as well as transmission and depolarization losses. Figure 4 shows a temporal trace of the picosecond pulse after the combiner. Imperfect polarizer transmission allows portions of each amplified replica to travel the wrong path through the combiner, resulting in pre- and post-pulses. The high transmission polarizers used in the combiner reduce these side pulses to about 1% of the main pulse. The pre-pulse intensity contrast was measured to be 82:1, while the post-pulse contrast is indiscernible due to the response of the photodiode.

Optimization of the combined output with increasing amplifier pump required adjustment of the HWP after the combiner to compensate for the change in energy distribution between the two picosecond replicas due to saturation. The B-integral associated phase difference between the pulse replicas changes with increased amplifier gain and must be compensated by slight adjustment of the QWP in the HC detector. This adjustment of the QWP starts to change the difference signal to the HC detector photodiodes, however the PI control immediately responds by shifting the piezo-mirror (and changing the OPD) in order to maintain the original difference signal between the HC photodiodes. The difficulty in optimization of these and other parameters with an energy stability of ~3% rms may account for the variance in the combination efficiency trends with increasing amplifier fluence.

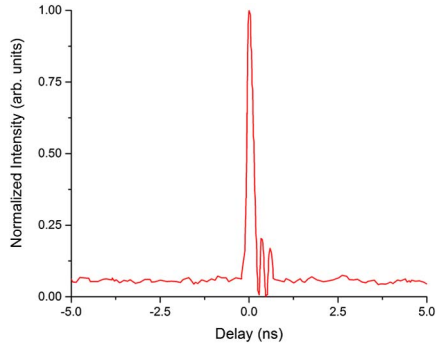

Fig. 4. Temporal trace of the picosecond pulse after combination using an 18.5 ps resolution photodiode and a 4 GHz oscilloscope.

In an attempt to isolate and quantify the fraction of combination efficiency loss primarily due to B-integral variation across the spatial profiles of the two recombined pulses, the fluence-dependent combination efficiency for 230 ps pulses is compared to that of 10 ns pulses, which were generated from the unseeded regenerative amplifier operating in cavity dumped mode. Since the B-integral accumulation for 10 ns pulses at these fluences is small, the additional loss in combination efficiency for 230 ps versus 10 ns pulses is largely due to B-integral effects and differences in saturation between the two temporally separated pulses (Fig. 3).

To maximize energy extraction, the seed beam profile overfilled both 10 mm diameter Nd:YAG amplifiers, and the resulting non-Gaussian beam profile was relay imaged to the pulse combiner. Asymmetry in the seed profile and diffraction in both 10 mm diameter amplifiers results in a complex non-ideal beam profile (inset Fig. 3). However, it is important to note that most high-energy lasers at the joule level and above exhibit flat-top and other profile shapes. This demonstration of 84% combination efficiency at three times the saturation fluence with a calculated peak B-integral of ~1.4 rad shows the robustness and scalability of the DPA technique to the joule level with other non-Gaussian profile shapes.

In summary, a record combined energy of 167 mJ (527 mJ equivalent) was obtained from, to the best of our knowledge, the first demonstration of DPA in a flashlamp-pumped amplifier system. A method to extend the benefits of active DPA and CBC to low-repetition rate, high-energy lasers is presented, which utilizes a secondary co-propagating CW laser to actively stabilize DPA for the pulses. Additionally, novel pulse splitter and combiner designs are demonstrated which minimize back-reflected energy, enable high transmission, and can be scaled to large aperture. The potential for DPA to provide energy scaling beyond the joule level is illustrated in the demonstration of 84% combination efficiency for two pulses at three times the gain saturation fluence of Nd:YAG. Comparable combination efficiency is expected scaling to larger aperture and energy, assuming similar levels of amplifier saturation and B-integral. Further scaling is possible by increasing the number of temporally delayed pulse replicas and/or the utilization of CBC in parallel amplifier channels.

Funding. Air Force Office of Scientific Research (AFOSR) (FA95501110001); Army Research Office (ARO) (W911-NF-0910500, W911-NF-1010491).

REFERENCES

1. D. Herrmann, L. Veisz, F. Tavella, K. Schmid, R. Tautz, A. Buck, V. Pervak, and F. Krausz, *Advanced Solid-State Photonics* (Optical Society of America, 2009), pp. 10–12.
2. A. Vaupel, N. Bodnar, B. Webb, L. Shah, and M. Richardson, Opt. Eng. **53**, 051507 (2013).
3. S. Zhou, F. W. Wise, and D. G. Ouzounov, Opt. Lett. **32**, 871 (2007).
4. A. Klenke, S. Hädrich, T. Eidam, J. Rothhardt, M. Kienel, S. Demmler, T. Gottschall, J. Limpert, and A. Tünnermann, Opt. Lett. **39**, 6875 (2014).
5. T. Eidam, J. Rothhardt, F. Stutzki, F. Jansen, S. Hädrich, H. Carstens, C. Jauregui, J. Limpert, and A. Tünnermann, Opt. Express **19**, 255 (2011).
6. S. Szatmari and P. Simon, Opt. Commun. **98**, 181 (1993).
7. L. Daniault, M. Hanna, D. N. Papadopoulos, Y. Zaouter, E. Mottay, F. Druon, and P. Georges, Opt. Express **20**, 21627 (2012).
8. F. Guichard, Y. Zaouter, F. Guichard, L. Daniault, M. Hanna, F. Morin, C. Honninger, E. Mottay, F. Druon, and P. Georges, Opt. Lett. **38**, 106 (2013).
9. T. Zhou, J. Ruppe, C. Zhu, I. Hu, and J. Nees, Opt. Express **23**, 7442 (2015).
10. M. Kienel, A. Klenke, T. Eidam, M. Baumgartl, C. Jauregui, J. Limpert, and A. Tünnermann, Opt. Express **21**, 29031 (2013).
11. T. W. Hansch and B. Couillaud, Opt. Commun. **35**, 441 (1980).
12. E. Seise, A. Klenke, S. Breitkopf, J. Limpert, and A. Tünnermann, Opt. Lett. **36**, 3858 (2011).
13. T. M. Shay, Opt. Express **14**, 12188 (2006).
14. T. M. Shay, V. Benham, J. T. Baker, A. D. Sanchez, D. Pilkington, and C. A. Lu, IEEE J. Sel. Top. Quantum Electron. **13**, 480 (2007).
15. M. Kienel, M. Müller, S. Demmler, J. Rothhardt, A. Klenke, T. Eidam, J. Limpert, and A. Tünnermann, Opt. Lett. **39**, 3278 (2014).
16. J. Pouysegur, F. Guichard, Y. Zaouter, M. Hanna, F. Druon, C. Hönninger, E. Mottay, and P. Georges, Opt. Lett. **40**, 5184 (2015).
17. F. Friebel, S. Ricaud, A. Pellegrina, M. Hanna, E. Mottay, P. Camy, J. L. Doualan, R. Moncorgé, P. Georges, F. Druon, and D. N. Papadopoulos, *Conference on Lasers and Electro-Optics—International Quantum Electronics Conference* (Optical Society of America, 2013), paper CA_10_4.
18. G. D. Goodno, C.-C. Shih, and J. E. Rothenberg, Opt. Express **18**, 25403 (2010).
19. S. Breitkopf, T. Eidam, A. Klenke, L. von Grafenstein, H. Carstens, S. Holzberger, E. Fill, T. Schreiber, F. Krausz, A. Tünnermann, I. Pupeza, and J. Limpert, Light Sci. Appl. **3**, e211 (2014).
20. S. W. Haan, J. D. Lindl, D. A. Callahan, D. S. Clark, J. D. Salmonson, B. A. Hammel, L. J. Atherton, R. C. Cook, M. J. Edwards, S. Glenzer, A. V. Hamza, S. P. Hatchett, M. C. Herrmann, D. E. Hinkel, D. D. Ho, H. Huang, O. S. Jones, J. Kline, G. Kyrala, O. L. Landen, B. J. MacGowan, M. M. Marinak, D. D. Meyerhofer, J. L. Milovich, K. A. Moreno, E. I. Moses, D. H. Munro, A. Nikroo, R. E. Olson, K. Peterson, S. M. Pollaine, J. E. Ralph, H. F. Robey, B. K. Spears, P. T. Springer, L. J. Suter, C. A. Thomas, R. P. Town, R. Vesey, S. V. Weber, H. L. Wilkens, and D. C. Wilson, Phys. Plasmas **18**, 051001 (2011).
21. N. Fleurot, C. Cavailler, and J. L. Bourgade, Fusion Eng. Des. **74**, 147 (2005).
22. E. S. Fulkerson, S. Telford, R. Deri, A. Bayramian, R. Lanning, E. Koh, K. Charron, and C. Haefner, *IEEE Pulsed Power Conference (PPC)* (IEEE, 2015), pp. 1–6.
23. X. Fu, Q. Liu, P. Li, Z. Sui, T. Liu, and M. Gong, Appl. Phys. Express **8**, 092702 (2015).
24. B. A. Reagan, C. Baumgarten, K. Wernsing, H. Bravo, M. Woolston, A. Curtis, F. J. Furch, B. Luther, D. Patel, C. Menoni, and J. J. Rocca, *CLEO* (Optical Society of America, 2014), paper SM1F.4.
25. A. Vaupel, N. Bodnar, B. Webb, L. Shah, M. Hemmer, E. Cormier, and M. Richardson, J. Opt. Soc. Am. B **30**, 3278 (2013).